The Growth of Silver on an Ordered Alumina Surface

K. Luo, X. Lai, C.-W. Yi, K. A. Davis, K. K. Gath, and D. W. Goodman*

Department of Chemistry, Texas A&M University, P.O. Box 30012, College Station, Texas 77842-3012

Received: September 8, 2004; In Final Form: November 24, 2004

The growth of Ag on an ordered Al_2O_3 surface was studied by low energy ion scattering spectroscopy (LEIS), scanning tunneling microscopy (STM), X-ray photoelectron spectroscopy (XPS), and temperature programmed desorption (TPD). Three-dimensional (3D) growth of Ag clusters was observed with STM and LEIS, with the cluster size increasing with Ag coverage. The XPS core level binding energies and the Auger parameters indicate a weak interaction between the Ag clusters and the Al_2O_3 support. Final state effects are determined to be the primary contribution to the Ag core level binding energy shift. Nonzero order kinetics was observed for Ag desorption in TPD with the Ag sublimation energy decreasing with decreasing cluster size.

Introduction

Alumina-supported silver catalysts are widely used for ethylene oxidation,[1,2] ethylene epoxidation,[3−5] formaldehyde oxidation,[6] methanol oxidation,[7,8] and NO_X reduction.[9,10] The surface morphology and the electronic/chemical properties of Ag/alumina then are very important with respect to the function and optimization of commercial catalysts. Model catalysts, prepared by growing Ag on ordered Al_2O_3 single crystals[11,12] or thin films on a Mo(110) substrate,[13] have been studied by temperature programmed desorption (TPD), atomic force microscopy (AFM), X-ray photoelectron spectroscopy (XPS), and isothermal measurements. Sticking probabilities near zero at 700 K and relatively small sublimation energies have been reported for Ag on α-$Al_2O_3(11\bar{2}0)$.[11] These authors also reported that Ag forms clusters on this surface as observed by AFM.[12] In addition, Rodriguez et al.[13] reported 0.4−0.6 eV Ag 3d XPS core level binding energy shifts and nonzero order desorption of Ag from an Al_2O_3 film supported on Mo(110).

In the present work, scanning tunneling microscopy (STM) and low energy ion scattering spectroscopy (LEIS) are used to study the growth mode of Ag on ordered Al_2O_3 films grown on Re(0001). From XPS, core level binding energies and Auger parameters are used to investigate the electronic properties of various Ag cluster sizes and interfacial reactions. The thermal stability and bonding between Ag and Al_2O_3 were also studied by XPS and TPD.

Experimental Section

The experiments were carried out in two ultrahigh vacuum (UHV) chambers. The first chamber was equipped with XPS, Auger electron spectroscopy (AES), LEIS, low energy electron diffraction (LEED), and TPD with a base pressure of 7×10^{-10} Torr. The XPS and LEIS spectra were collected using a concentric hemispherical analyzer (PHI, SCA 10-360). For the XPS data, the experimental error is ±0.1 eV for the Ag 3d core level and ±0.2 eV for the Ag M_5VV Auger transitions due to the relatively broad peaks. The TPD experiments were carried out using a closed-coupled (∼2 mm), line-of-sight quadruple mass spectrometer (QMS) with a linear sample heating rate of 3 K/s. The second chamber was equipped with STM (Omicron-1), XPS, AES, and LEED, with a base pressure of 1×10^{-10} Torr. The STM images were collected in a constant current topography (CCT) mode.

The Re(0001) single crystal was spot-welded to high-purity tantalum wires connected to two copper leads. The sample could be heated to 1500 K by resistive heating, to 2400 K by electron-beam (e-beam) heating, and cooled to 90 K using liquid nitrogen. The sample temperature was measured using a W/Re (Type C) thermocouple spot-welded to the back of the crystal. The Re crystal was cleaned by e-beam heating to 2300 K until no contamination was detected by AES and XPS, and a sharp 1×1 hexagonal LEED pattern was evident.

The alumina film was synthesized[14] by exposing the Re(0001) surface to Al vapor in a O_2 pressure of 1×10^{-5} Torr at 300 K with a subsequent anneal to 1000 K in O_2 (1×10^{-6} Torr). Afterward, the film was annealed to 1000 K in UHV, and then characterized by XPS, AES, LEIS, LEED, and STM. XPS and AES studies showed the film to be fully oxidized. A hexagonal 1×1 LEED pattern was observed for films with thicknesses of 1.0−10 nm. STM showed the films to be exceptionally flat (with a roughness of less than a few angstroms). The film thickness was estimated by attenuation of the XPS Re 4f core level peak intensity, assuming a mean free path for the Re 4f photoelectrons in Al_2O_3 of 2.8 nm.

For the Ag film deposition, a Ag doser was made of high-purity Ag wires (99.99%) wrapped around a Ta filament. The deposition rate of Ag, calibrated via TPD and AES of Ag on Re(0001), was 1 monolayer (ML) per 400 s.

Results and Discussion

Ag/Al_2O_3 Growth Mode. The growth mode of metals on oxides is of considerable importance in the synthesis of oxide-supported metal clusters as models for studies in heterogeneous catalysis. The three-dimensional (3D) images in Figure 1 show the growth of 0.05, 0.5, 1.0, and 2.0 ML Ag on alumina at 300 K. At relatively small coverages, that is, 0.05 ML, Ag forms very small clusters, ranging from 1 to 3.5 nm in diameter, with heights of 0.4−1.2 nm, hemispherical in shape. Thereafter, the size of the Ag clusters increases with increasing Ag coverage. At 0.5 ML, the clusters are 4−8 nm in diameter, with heights of 1.0−3.0 nm. At 1.0 ML, Ag clusters range from 4.5 to 9

* To whom correspondence should be addressed. Fax: (979) 845-6822. E-mail: goodman@mail.chem.tamu.edu.

10.1021/jp045948k CCC: $30.25
Published on Web 02/08/2005

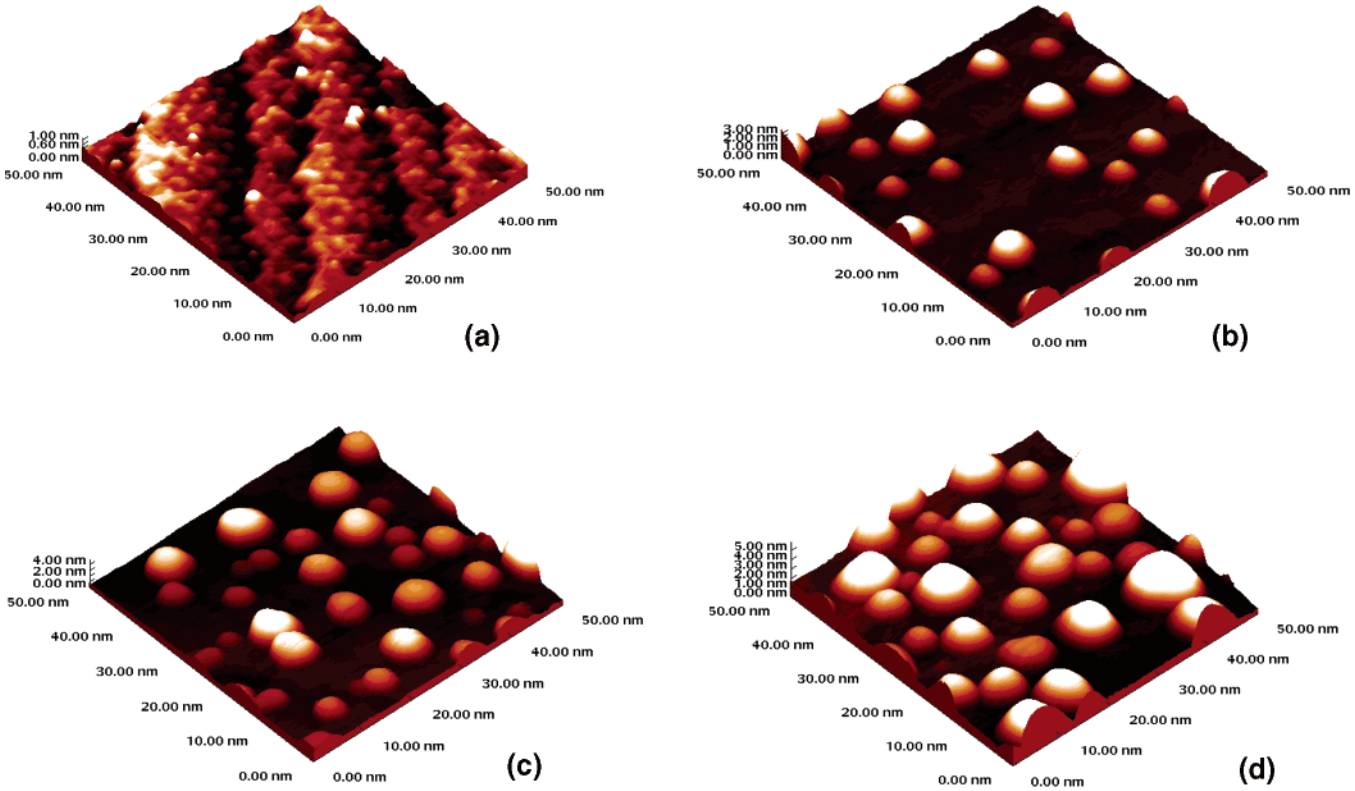

Figure 1. Constant current topography (CCT) STM images (50 nm × 50 nm) of Ag on Al_2O_3/Re(0001) at 300 K: (a) 0.05 ML; (b) 0.5 ML; (c) 1.0 ML; and (d) 2.0 ML.

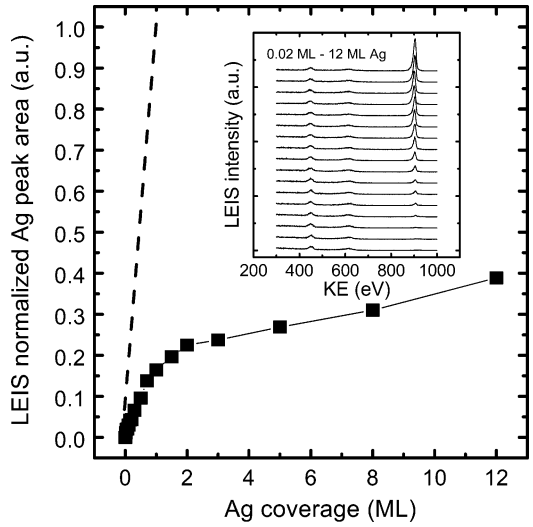

Figure 2. LEIS Ag peak area, normalized to that for 1.0 ML Ag on Re(0001), as a function of Ag coverage on Al_2O_3/Re(0001). The inset is the LEIS spectra as a function of Ag coverage.

nm, with heights of 1.2−4.2 nm. At 2.0 ML, the Ag clusters are 4.5−10 nm in diameter, with heights of 1.7−5.0 nm. In magnified STM images (not shown) of 2.0 ML Ag coverage, the clusters grow randomly on the surface with no preference for the step edges or terraces. From the STM data, a three-dimensional (3D) growth mode of Ag clusters is clearly observed from 0.05 to 2 ML, with the cluster density and volume increasing with coverage.

LEIS was also used to study the Ag cluster growth mode. In the inset of Figure 2, LEIS spectra are shown as a function of Ag coverage. In the bottom spectrum for zero Ag coverage, the two LEIS features at 448 and 615 eV are assigned to O and Al. The intensity of these features decreases slowly with increasing Ag coverage. A feature at 906 eV appears following deposition of Ag. In Figure 2, the area of the Ag LEIS feature, normalized to that for 1.0 ML Ag on Re(0001), is plotted as a function of Ag coverage. The dashed line corresponds to a two-dimensional (or layer-by-layer) growth mechanism. The actual data deviate from the dashed line and are more characteristic of 3D Ag growth.[15,16] The LEIS and STM data are strong evidence for a 3D-cluster growth mode for Ag on the alumina thin film/Re(0001) at 300 K.

The growth mode of a metal on an oxide surface is determined by minimization of the surface free energy of the oxide (γ_{ox}), the deposited metal (γ_m), and the interfacial free energy ($\gamma_{m/ox}$).[17−19] If the γ_{ox} is less than the sum of γ_m and $\gamma_{m/ox}$, the oxide surface tends to maximize its exposed area, leading to a Volmer−Weber (VW) or 3D metal growth mode. For the converse, layer-by-layer or layer-followed-by-cluster growth occurs. In the present studies, Ag has a surface free energy of ~1.3 J/m^2.[20,21] The surface free energy of alumina is approximately 0.4 J/m^2 smaller than that of Ag.[22] Due to the weak interaction between Ag and alumina (described later in the text), $\gamma_{m/o}$ is estimated to be very small. Thus, to minimize the surface free energy, the exposed alumina surface area will be maximized; that is, Ag should grow three-dimensionally on alumina. The experimental results show this to be the case.

Interfacial Interaction and Electronic Properties. XPS core level binding energy shifts as a function of cluster size have been reported for many metal/oxide systems. Differentiation of the relative contribution of initial and final state effects to core level binding energy (BE) shifts inevitably is an issue. In Figure 3a and b, the Ag $3d_{5/2}$ core level binding energy and Ag M_5VV Auger transition binding energy are plotted as a function of Ag coverage at 300 K. Both Ag $3d_{5/2}$ and M_5VV Auger binding energies shift to a higher BE with decreasing Ag coverage. At 0.04 ML Ag coverage, the Ag 3d core level and M_5VV Auger peak positions are higher than the bulk Ag value by 0.9 and

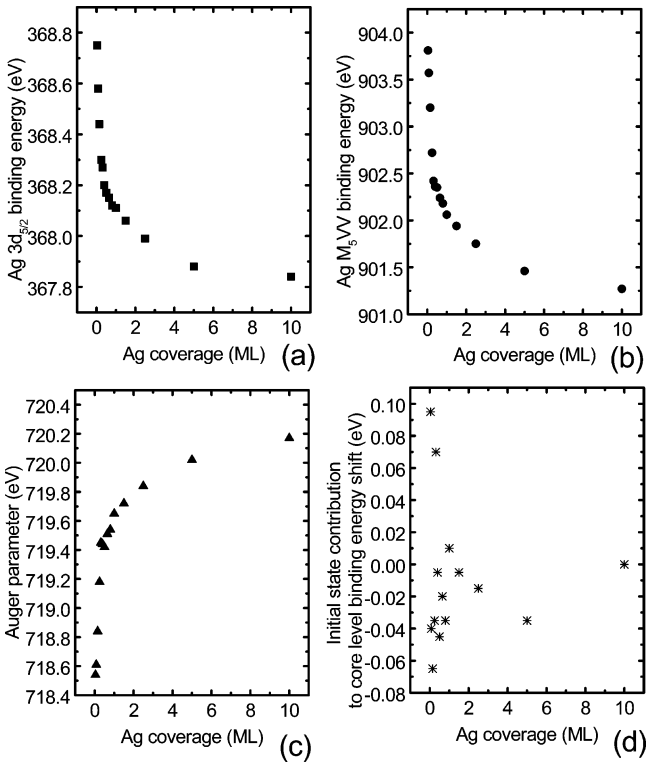

Figure 3. (a) XPS Ag $3d_{5/2}$ core level binding energy; (b) Ag M_5VV Auger peak binding energy; (c) Auger parameter; and (d) initial state contribution to the core level binding energy shifts as a function of Ag coverage on Al_2O_3/Re(0001) at 300 K.

2.5 eV, respectively. At 10.0 ML Ag coverage, each approaches the bulk Ag value.

Regarding the initial and finial state contributions to the core level BE shifts, Mason, Bagus, and Parmegiani concluded that initial state effects, such as the atomic coordination or metal−surface interaction, dominate the shifts for small metal clusters on poorly conducting surfaces.[23−25] However, Egelhoff and Tibbetts suggested that final state screening, that is, relaxation effects, is the main cause of binding energy shifts for metal clusters with varying size.[26,27] Wertheim claimed that Coulombic effects in the final state contribute primarily to the binding energy shift for metal clusters on poorly conductive substrates such as amorphous carbon.[28−30]

In the early 1970s, Wagner first introduced the concept of the Auger parameter (α)[31,32] to study photoemission binding energy shifts. The Auger parameter that is widely used currently is defined[33−35] as

$$\alpha = E_b(C') + E_k(C'C''C''') \quad (1)$$

where $E_b(C')$ is the core level (C′) binding energy and $E_k(C'C''C''')$ is the kinetic energy of the Auger transitions from the C′, C″, and C‴ core levels, respectively. By assuming equal binding energy shifts and identical relaxation mechanisms for all three core levels, the change in the Auger parameter ($\Delta\alpha$) is approximately twice the final state effects (ΔR),[36,37] including extra-atomic relaxation and the Coulombic energy, and is written as

$$\Delta\alpha = 2\Delta R \quad (2)$$

This equation offers a direct way to evaluate the contribution of final state effects, and thus to separate initial and final state contributions to the observed binding energy shifts.

Experimentally, due to the wide application of Al and Mg Kα X-ray sources, most Auger transition peaks come from C′VV or C′C″V excitation, rather than C′C″C‴ excitation. Validation of the two assumptions in eq 2 for transitions involving the valence band strongly determines the limitation of its application. Moretti[35] and Wertheim[37] pointed out that the validation of the two assumptions is fully dependent on the structure and depth of the valence band. In the case of atomic-like Auger transitions, like O KVV, Pt MVV, or Sn MNN, etc., the assumptions are valid. Nevertheless, due to the large delocalization of valence band and changes in screening effects between core holes and valence holes, some band-like Auger transitions should not be used to extract the Auger parameter. In our study of the growth of Ag on ultrathin Al_2O_3 films (∼30 Å) using a Mg Kα source, Ag has an intense and sharp Auger M_5VV (3d−4d) transition feature in the XPS spectra. As a 4d metal, Ag has been studied experimentally and theoretically in terms of its validity with respect to the Auger parameter approximation.[16,28,38,39] In Ag growth on amorphous carbon[28] and TiO_2(110) single-crystal surfaces,[16] the core level binding energies shift systematically with the centroid of the 4d valence band. In the present work, the valence band was monitored (not shown) and its centroid was observed to shift in concert with the core level features. From Kleiman et al.'s work,[38,39] the 4d valence holes of all 4d metals (except Pd) have the same relaxation in the final state as the 3d core holes. Therefore, both assumptions in eq 2 are valid for Ag M_5VV.

Using eq 1, the Auger parameter (α) can be calculated from the data in Figure 3a and b and is plotted as a function of Ag coverage in Figure 3c. The Auger parameter decreases with decreasing Ag coverage and shifts in the opposite direction from the 3d core level and MVV transitions. The shift is on the order of ∼1.6 eV. According to eq 2, the final state effect contribution to the core level BE shift, that is, half of the change of the Auger parameter ($\Delta\alpha/2$), can be estimated from the data in Figure 3c. Subtracting the final state contribution from the core level BE shift, the initial state effect contribution can be calculated and is plotted as a function of Ag coverage in Figure 3d. Essentially the initial state contribution to the Ag core level BE shift (0.9 eV) is very small (within ±0.1 eV) from very low (0.04 ML) to high (10.0 ML) Ag coverages. These data clearly delineate the importance of final state contributions to core level BE shifts. In addition, in the study of the alumina Al 2s and O 1s (not shown), the binding energies show no shifts until 2.0 ML Ag. Up to 10.0 ML, both Al 2s and O 1s shift toward a lower binding energy by ∼0.2 eV, which is interpreted as metal cluster screening on the alumina film.[40] These results indicate a very weak interaction between Ag clusters and the Al_2O_3 thin film and suggest that the origin of the Ag core level BE shift is a final state effect.

Another important approach for differentiating initial and final state effects was shown in the work of Moretti.[35] Using an electrostatic model, the assumptions of similar initial state effects, and the approximations used to derive eq 2, a plot of Auger kinetic energy $E_k(C'C''C''')$ versus core level binding energy $E_b(C')$ obtained from metal XPS spectra for different size of clusters, that is, a Wagner plot, should have a linear relationship with a slope of −3.[35,36] This method can be used to differentiate the initial and final state effects in core level BE shifts. Because the assumptions for eq 2 are all met for Ag, the Wagner plot is also employed here to study the initial and/or final state effect contributions to the binding energy shifts. In Figure 4, the Ag M_5VV kinetic energy is plotted as a function of Ag $3d_{5/2}$ binding energy. The linear fit (solid line)

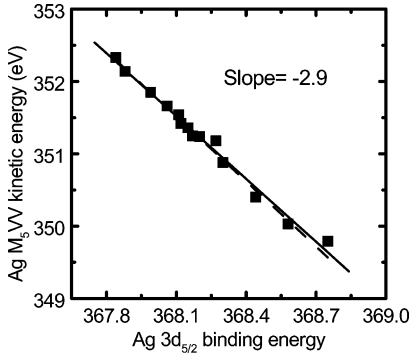

Figure 4. A Wagner plot of Ag M_5VV kinetic energy versus Ag $3d_{5/2}$ binding energy as a function of Ag coverage.

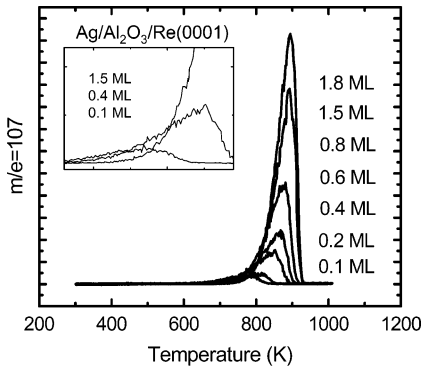

Figure 5. TPD spectra of Ag as a function of Ag coverage.

yields a straight line with a slope of −2.9, which is very close to the dashed line with a slope of −3. The similarities in the slopes of the solid and dashed lines strongly support the origin of the core level BE shifts in Figure 3a being final state effects.

Temperature Programmed Desorption of Ag. Figure 5 shows a series of TPD spectra of Ag on Al_2O_3/Re(0001) as a function of the Ag coverage (0.1−1.8 ML). The peak profiles are asymmetric with the leading edges moving toward higher temperatures with increasing Ag coverage (shown in the inset). On the low-temperature side of the peaks, the desorption rate is higher for low coverages as compared to high coverages. On the high-temperature side, the desorption rate drops sharply. Our results are consistent with studies of Ag on α-Al_2O_3 single crystals and alumina thin films on Ru and Mo[11,13] in that the order of the desorption is fractional rather than zero. In Monte Carlo simulations[41] of the TPD spectra, the various metal cluster sizes are considered as finite islands. With increasing coverage, the average cluster size increases and the peak maximum shifts toward higher temperature. At a certain temperature, the desorption rate increases significantly and desorption occurs within a narrow temperature range. Thereafter, the desorption rate falls rapidly after reaching the peak desorption temperature, giving rise to a sharp drop in the desorption rate on the high-temperature side of the desorption peak.

The sublimation energies (E_{sub}) of the Ag clusters as a function of coverage, extracted using the leading edge analysis, are plotted in Figure 6. The E_{sub}'s drop to approximately 20 kcal/mol at a Ag coverage of 0.2 ML. The sublimation energy increases with increasing coverage until the bulk value is reached at approximately 3.0 ML. The increase in the number of low-coordinated Ag atoms in small clusters relative to larger clusters combined with a stronger Ag−Ag as compared to Ag−Al_2O_3 interaction likely are responsible for the large variation in the Ag sublimation energies.

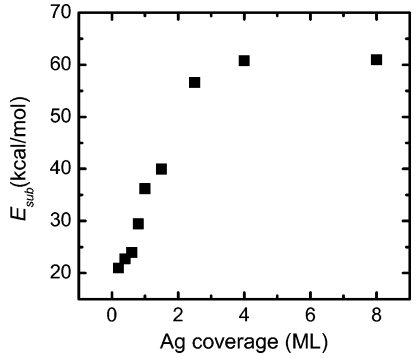

Figure 6. Cluster sublimation energies (E_{sub}) deduced using the leading edge analysis of TPD spectra of Figure 5.

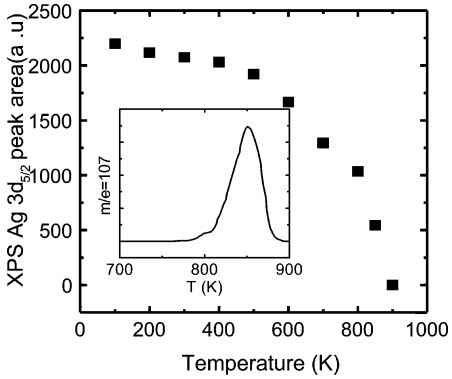

Figure 7. XPS Ag $3d_{5/2}$ peak intensity as a function of temperature for a 0.1 ML Ag/Al_2O_3/Re(0001). The inset is the corresponding TPD spectrum at the same Ag coverage.

Thermal Sintering. Thermal sintering of oxide-supported metal clusters has been reported for various metal-oxide systems.[16,19,40,42] In the present study, this effect was studied with XPS and TPD. 0.1 ML Ag was deposited on the Al_2O_3 film at 100 K, annealed, after which XPS spectra were collected at 100 K. In Figure 7, the XPS Ag $3d_{5/2}$ peak area intensities are plotted as a function of temperature. The inset is the TPD spectrum of the corresponding Ag coverage. From 100 to 500 K, the Ag peak intensity decreases slightly, consistent with cluster sintering. From 500 to 800 K, although the temperature is still well below the desorption temperature of Ag, the peak intensity falls rapidly showing that significant sintering of the Ag clusters occurs well before desorption. After 800 K, the peak intensity falls concurrently with the desorption of Ag until the surface is Ag-free.

To investigate the interfacial interactions upon annealing, the Ag $3d_{5/2}$ binding energy, Ag M_5VV binding energy, Auger parameter, and initial state contribution to Ag core level BE shift at 0.1 ML Ag were studied. The same methodology used in Figure 3 was employed with the anneal temperature as the variable rather than Ag coverage. It was observed that Ag core level and Auger transition binding energies shift to lower binding energies with increasing temperature, reaching the bulk value near 800 K. The Auger parameter, on the other hand, shifts toward higher binding energies with increasing temperature. The initial state contribution to the core level BE shift, caused by the temperature-induced sintering, is less than ∼0.1 eV. Additionally, a Wagner plot (not shown) of the Ag M_5VV kinetic energy versus the Ag $3d_{5/2}$ binding energy indicates a linear relationship with a slope of −3.1. No large binding energy shifts were observed on either O or Al core level peaks. Therefore, all of the data indicate that the temperature-induced core level BE shifts are due primarily to final state effects.

Conclusions

As an important model catalyst, Ag/Al_2O_3 ultrathin film/Re(0001) was systematically studied by STM, LEIS, XPS, and TPD. At 300 K, three-dimensional Ag growth was observed. The use of the Auger parameter and Wagner plots allows separation of initial and final state effects in core level binding energy shifts for Ag clusters of various sizes. Final state effects are concluded to be primarily responsible for the core level binding energy shifts. No strong interfacial interaction between Ag and alumina was apparent between 100 K and the desorption temperature of Ag. TPD data indicate weak bonding between Ag and alumina within the small cluster regime.

Acknowledgment. We would like to acknowledge support of this work by the Department of Energy, Office of Basic Energy Sciences, Division of Chemical Sciences, and the Robert A. Welch Foundation.

References and Notes

(1) Corner, P. T.; Kovenklioglu, S.; Shelly, D. C. *Appl. Catal.* **1991**, *71*, 247.
(2) Mao, C.-F.; Vannice, M. A. *Appl. Catal., A* **1995**, *122*, 61.
(3) Minahan, D. M.; Hoflund, G. B. *J. Catal.* **1996**, *158*, 109.
(4) Hoflund, G. B.; Minahan, D. M. *Nucl. Instrum. Methods Phys. Res., Sect. B* **1996**, *118*, 517.
(5) Bukhtiyarov, V.; Prosvirin, I. P.; Kvon, R. I.; Goncharova, S. N.; Bal'zhinimaev, B. S. *J. Chem. Soc., Faraday Trans.* **1997**, *93*, 2323.
(6) Mao, C.-F.; Vannice, M. A. *J. Catal.* **1995**, *154*, 230.
(7) Wang, J.-A.; Aguilar-Rios, G.; Wang, R. *Appl. Surf. Sci.* **1999**, *147*, 44.
(8) Cordi, E. M.; Falconer, J. L. *Appl. Catal., A* **1997**, *151*, 179.
(9) Takagi, K.; Kobayashi, T.; Ohkita, H.; Mizushima, T.; Kakuta, N.; Abe, A.; Yoshida, K. *Catal. Today* **1998**, *45*, 123.
(10) Abe, A.; Aoyama, N.; Sumiya, S.; Kakuta, N.; Yoshida, K. *React. Kinet. Catal. Lett.* **1998**, *65*, 139.
(11) Van Campen, D. G.; Hrbek, J. *J. Phys. Chem.* **1995**, *99*, 16389.
(12) Beitel, G.; Markert, K.; Wiechers, J.; Hrbek, J.; Behm, R. J. In *Spring Series in Surface Science*; Umbach, E., Freund, H.-J., Eds.; Springer-Verlag: Berlin, Heidelberg, 1993; Vol. 33.
(13) Rodriguez, J. A.; Kuhn, M.; Hrbek, J. *J. Phys. Chem.* **1996**, *100*, 18240.
(14) Lai, X.; Chusuei, C. C.; Luo, K.; Guo, Q.; Goodman, D. W. *Chem. Phys. Lett.* **2000**, *330*, 226.
(15) Diebold, U.; Pan, J.-M.; Madey, T. E. *Phys. Rev. B* **1993**, *47*, 3868.
(16) Luo, K.; St. Clair, T. P.; Lai, X.; Goodman, D. W. *J. Phys. Chem. B* **2000**, *104*, 3050.
(17) Bauer, E. *Z. Kristallogr.* **1958**, *110*, 372.
(18) Egelhoff, W. F., Jr. In *Ultathin Magnetic Structures I, An Introduction to Electronic, Magnetic, and Structural Properties*; Bland, J. A. C., Heinrich, B., Eds.; Springer-Verlag: Berlin, 1994.
(19) Persaud, R.; Madey, T. E. In *Growth and Properties of Ultrathin Epitaxial Layers*; King, D. A., Woodruff, D. P., Eds.; Elsevier Science B. V.: New York, 1997.
(20) Mezey, L. Z.; Giber, J. *Jpn. J. Appl. Phys.* **1982**, *21*, 1569.
(21) Vitos, L.; Ruban, A. V.; Skriver, H. L. *Philos. Mag. B* **1998**, *78*, 487.
(22) Overbury, S. H.; Bertrand, P. A.; Somorjai, G. A. *Chem. Rev.* **1975**, *75*, 547.
(23) Mason, M. G. *Phys. Rev. B* **1983**, *27*, 748.
(24) Parmigiani, F.; Kay, E.; Bagus, P. S. *J. Electron Spectrosc. Relat. Phenom.* **1985**, *36*, 257.
(25) Bagus, P. S.; Brundle, C. R.; Pacchioni, G.; Parmegiani, F. *Surf. Sci. Rep.* **1993**, *19*, 265.
(26) Egelhoff, W. F., Jr.; Tibbetts, G. G. *Phys. Rev. B* **1979**, *19*, 5028.
(27) Egelhoff, W. F., Jr.; Tibbetts, G. G. *Solid State Commun.* **1979**, *29*, 53.
(28) Wertheim, G. K.; DiCenzo, S. B.; Youngquist, S. E. *Phys. Rev. Lett.* **1983**, *51*, 2310.
(29) Wertheim, G. K.; DiCenzo, S. B.; Buchanan, D. N. E. *Phys. Rev. B* **1986**, *33*, 5384.
(30) Wertheim, G. K. *Z. Phys. D: At., Mol. Clusters* **1989**, *12*, 319.
(31) Wagner, C. D. *Anal. Chem.* **1972**, *44*, 967.
(32) Wagner, C. D. *Faraday Discuss. Chem. Soc.* **1975**, *60*, 291.
(33) Gaarenstroom, S. W.; Winograd, N. *J. Chem. Phys.* **1977**, *67*, 3500.
(34) Wagner, C. D.; Gale, L. H.; Raymond, R. H. *Anal. Chem.* **1979**, *51*, 466.
(35) Moretti, G. *J. Electron Spectrosc. Relat. Phenom.* **1998**, *95*, 95.
(36) Wu, Y.; Garfunkel, E.; Madey, T. E. *J. Vac. Sci. Technol., A* **1996**, *14*, 1662.
(37) Wertheim, G. K. *Phys. Rev. B* **1987**, *36*, 9559.
(38) Kleiman, G. G.; Landers, R.; Nascente, P. A. P.; de Castro, S. G. C. *Phys. Rev. B* **1992**, *46*, 4405.
(39) Kleiman, G. G.; Landers, R.; Nascente, P. A. P.; de Castro, S. G. C. *Surf. Sci.* **1993**, *287/288*, 798.
(40) Luo, K.; Kim, D. Y.; Goodman, D. W. *J. Mol. Catal. A* **2001**, *167*, 191.
(41) Masel, R. I. *Principles of Adsorption and Reaction on Solid Surfaces*; Wiley Series in Chemical Engineering; Wiley: New York, 1996.
(42) Zhang, L.; Persaud, R.; Madey, T. E. *Phys. Rev. B* **1997**, *56*, 10549.